Research Article | Vol. 25, No. 22 | 30 Oct 2017 | OPTICS EXPRESS 26600
Optics EXPRESS

Effects of the gap slope on the distribution of removal rate in Belt-MRF

DEKANG WANG,[1,2] HAIXIANG HU,[1,*] LONGXIANG LI,[1] YANG BAI,[1] XIAO LUO,[1] DONGLIN XUE,[1] AND XUEJUN ZHANG[1]

[1]*Key Laboratory of Optical System Advanced Manufacturing Technology, Changchun Institute of Optics, Fine Mechanics and Physics, Chinese Academy of Sciences, Changchun, Jilin 130033, China*
[2]*University of Chinese Academy of Sciences, Beijing 100049, China*
**hhx@ciomp.ac.cn*

Abstract: Belt magnetorheological finishing (Belt-MRF) is a promising tool for large-optics processing. However, before using a spot, its shape should be designed and controlled by the polishing gap. Previous research revealed a remarkably nonlinear relationship between the removal function and normal pressure distribution. The pressure is nonlinearly related to the gap geometry, precluding prediction of the removal function given the polishing gap. Here, we used the concepts of gap slope and virtual ribbon to develop a model of removal profiles in Belt-MRF. Between the belt and the workpiece in the main polishing area, a gap which changes linearly along the flow direction was created using a flat-bottom magnet box. The pressure distribution and removal function were calculated. Simulations were consistent with experiments. Different removal functions, consistent with theoretical calculations, were obtained by adjusting the gap slope. This approach allows to predict removal functions in Belt-MRF.

OCIS codes: (220.0220) Optical design and fabrication; (220.4610) Optical fabrication; (220.5450) Polishing

References and links

1. D. Golini, G. Schneider, P. Flug, and M. Demarco, "The Ultimate Flexible optics manufacturing technology: Magnetorheological Finishing," Opt. Photonics News **12**(10), 20–24 (2001).
2. K. Ren, X. Luo, L. Zheng, Y. Bai, L. Li, H. Hu, and X. Zhang, "Belt-MRF for large aperture mirrors," Opt. Express **22**(16), 19262–19276 (2014).
3. W. Huang, Y. Zhang, J. Hel, Y. Zheng, Q. Luo, J. Hou, and Z. Yuan, "Research on the magnetorheological finishing (MRF) technology with dual polishing heads," Proc. SPIE **9281**, 92811U (2014).
4. C. Maloney, J. P. Lormeau, and P. Dumas, "Improving low, mid and high-special frequency errors on advanced aspherical and freeform optics with MRF," Proc. SPIE **10009**, 100090R (2016).
5. J. C. Lambropoulos, F. Yang, and S. D. Jacobs, "Toward a mechanical mechanism for material removal in magnetorheological finishing," in *Optical Fabrication and Testing Workshop* (Optical Society of America, 1996), pp. 150–153.
6. A. B. Shorey, S. D. Jacobs, W. I. Kordonski, and R. F. Gans, "Experiments and observations regarding the mechanisms of glass removal in magnetorheological finishing," Appl. Opt. **40**(1), 20–33 (2001).
7. J. E. Degroote, A. E. Marino, J. P. Wilson, A. L. Bishop, J. C. Lambropoulos, and S. D. Jacobs, "Removal rate model for magnetorheological finishing of glass," Appl. Opt. **46**(32), 7927–7941 (2007).
8. C. Miao, J. C. Lambropoulos, and S. D. Jacobs, "Process parameter effects on material removal in magnetorheological finishing of borosilicate glass," Appl. Opt. **49**(10), 1951–1963 (2010).
9. W. I. Kordonski, D. Golini, P. Dumas, and S. Hogan, "Magnetorheological suspension-based finishing technology," Proc. SPIE **3326**, 527–535 (1998).
10. A. B. Shorey, "Mechanisms of material removal in magnetorheological finishing of glass," Ph.D. dissertation (University of Rochester, 2000).
11. F. Zhang, J. Yu, and X. Zhang, "Magnetorheological finishing technology," Opt. Precis. Eng. **7**(5), 1–8 (1999).
12. Y. Dai, C. Song, X. Peng, and F. Shi, "Calibration and prediction of removal function in magnetorheological finishing," Appl. Opt. **49**(3), 298–306 (2010).
13. W. Kordonski and S. Gorodkin, "Material removal in magnetorheological finishing of optics," Appl. Opt. **50**(14), 1984–1994 (2011).
14. H. Yang, J. He, W. Huang, and Y. Zhang, "Spot breeding method to evaluate the determinism of magnetorheological finishing," Opt. Eng. **56**(3), 035101 (2017).
15. F. W. Preston, "The theory and design of plate glass polishing machines," J. Soc. Glass Technol. **11**, 214–256 (1927).

#305002 https://doi.org/10.1364/OE.25.026600
Journal © 2017 Received 18 Aug 2017; revised 2 Oct 2017; accepted 3 Oct 2017; published 17 Oct 2017

Optics EXPRESS

16. M. Das, V. K. Jain, and P. S. Ghoshdastidar, "Fluid flow analysis of magnetorheological abrasive flow finishing (MRAFF) process," Int. J. Mach. Tools Manuf. **48**, 415–426 (2008).
17. J. Engmann, C. Servais, and A. S. Burbidge, "Squeeze flow theory and applications to rheometry: A review," J. Non-Newt. Fluid Mech. **132**, 1–27 (2005).
18. M. Schinhaerl, C. Vogt, A. Geiss, R. Stamp, P. Sperber, L. Smith, G. Smith, and R. Rascher, "Forces acting between polishing tool and workpiece surface in magnetorheological finishing," Proc. SPIE **7060**, 706006 (2008).
19. J. C. Lambropoulos, C. Miao, and S. D. Jacobs, "Magnetic field effects on shear and normal stresses in magnetorheological finishing," Opt. Express **18**(19), 19713–19723 (2010).
20. H. M. Laun, C. Gabriel, and G. Schmidt, "Primary and secondary normal stress differences of a magnetorheological fluid (MRF) up to magnetic flux densities of 1 T," J. Non-Newtonian Fluid Mech. **148**, 47–56 (2008).
21. Y. Bai, L. Li, D. Xue, and X. Zhang, "Rapid fabrication of a silicon modification layer on silicon carbide substrate," Appl. Opt. **55**(22), 5814–5820 (2016).
22. *http://www.tekscan.com*.

1. Introduction

Magnetorheological finishing (MRF) is a sub-aperture polishing method that is used in optical fabrication. It has been widely applied to polishing various optical materials; some advantages of this method are its high reliability and the fact that it incurs zero wear and no sub-surface damage [1]. The MRF method uses a magnetorheological (MR) fluid that typically consists of magnetic carbonyl iron particles, non-magnetic polishing abrasives, carrier fluids, and stabilizers. The MR fluid stiffens in the presence of a high-gradient magnetic field, to form ribbon protrusions as a polishing tool. A strong shearing force is generated when the ribbon flows into a small converging gap between the workpiece and the wheel, leading to the removal of surface material. However, the volume removal rate (VRR) of material still needs to be improved for large-aperture optics. Larger VRR requires the wheel to be larger. In general, the wheel should be several times larger than the produced spot, which limits the method's applicability to large optical processing.

Belt magnetorheological finishing (Belt-MRF), a type of magnetorheological finishing, was first proposed by Ren in 2014 [2]. Belt-MRF uses a belt instead of a wheel as a carrier of the MR fluid flow, as shown in Fig. 1. It can extend the length of the spot by uniformly increasing the length of the magnet box.

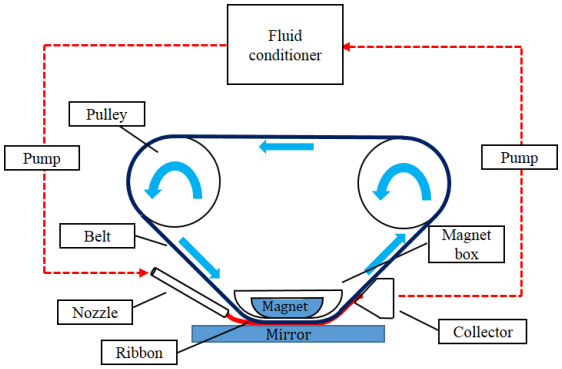

Fig. 1. Schematic of the Belt-MRF method.

More specifically, the Belt-MRF approach uses a belt that enwraps a permanent magnet box with a certain radius. The effect is equivalent to that of using a polishing wheel with the same radius of curvature. In addition, this setup increases the relative speed between the workpiece and the ribbon by increasing the line speed of the belt, which is limited for large wheels in conventional MRF. As to the large MRF wheels, the increasing speed will induce more deformation of the wheel and more wear of the rotation shaft caused by the centrifugal force. Thus make it difficult to maintain a high stability of the polishing gap (ordinarily

Optics EXPRESS

required within 10μm-class accuracy). While in Belt-MRF, the magnet box is mechanically fastened, it is promising to produce a larger polishing area and a higher material removal rate.

Removal spots are used in different polishing applications, depending on their shapes [3]. Large removal spots, with high removal rate, are used in large-aperture optics. Small removal spots are suitable for polishing small-aperture optics. Uniform removal spots, with "platform" removal rate, are used in fabrication of semiconductor silicon wafers. In 2016, QED presented a combination of different-sized spots for figuring and smoothing [4]. In particular, the removal function in Belt-MRF differs from that in conventional MRF. Because the belt's shape is determined by the shape of the magnet box rather than the wheel, Belt-MRF is promising for designing removal spots with a variety of shapes. For this, it is necessary to establish a removal model of Belt-MRF.

As to MRF, two aspects of the removal function model have been addressed recently. The VRR in MRF was studied in terms of the technical parameters of the polishing process [5–8]. Other studies addressed the removal distribution model of MRF. Kordonski [9] and Shorey [10] calculated the shear stress by measuring the normal pressure distribution of the removal spot, and then demonstrated that the shear stress and the removal function are consistent. Zhang [11] calculated the normal pressure, consisting of the hydrodynamic pressure and magnetic pressure, and compared it with the removal function. Dai [12] established a calibrated model by scaling the removal function with different materials in use. Kordonski [13] later proposed another removal rate model based on the particle force, which was in good qualitative and quantitative agreements with experimental results.

Although many attempts were undertaken to determine the effects of technical parameters on the removal process and to determine how the forces are related to the removal of material, designing a certain removal function, especially for long-and-narrow Belt-MRF situations, remains difficult. In general, no concise model has been proposed so far to explain the mechanism of material removal in Belt-MRF, to calibrate the model parameters, and to predict the removal function.

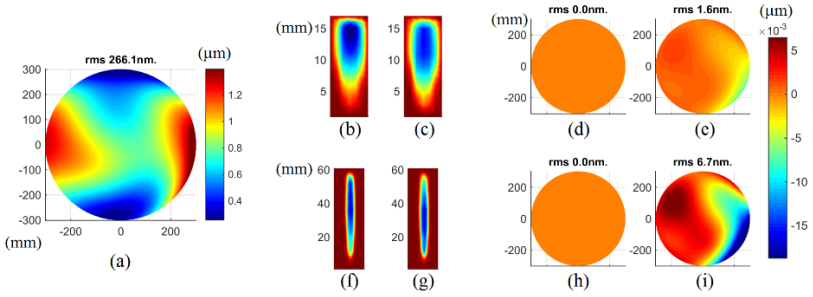

Fig. 2. The simulation polishing results on spot distribution differences of MRF and Belt-MRF (a) Initial surface error map of ⌀600mm flat [2]. (b) Aimed MRF spot, used to calculate dwell time. (c) Actual MRF spot, with distribution changed linearly. (d) Simulative polishing residual map, using aimed MRF spot. (e) Simulative polishing residual map, using actual MRF spot. (f) Aimed Belt-MRF spot [2], used to calculate dwell time. (g) Actual Belt-MRF spot, with distribution changed linearly. (h) Simulative polishing residual map, using aimed Belt-MRF spot. (i) Simulative polishing residual map, using actual Belt-MRF spot.

As to such a long-and-narrow spot, the polishing residual is not mainly affected by VRR only, but also the material removal distribution. In Fig. 2, a set of simulative polishing results is shown with equal-VRR MRF and Belt-MRF spots. The initial surface error map in Fig. 2(a) is same as Fig. 23 in Ren's work [2], while the aimed Belt-MRF spot (~53mm long) in Fig. 2(f) is same as Fig. 20 in Ren's work [2] as well. After simulative convergence, the residual errors (h) RMS <0.1nm. If once the material removal distribution changed from (f) into (g) unexpectedly, the residual errors (i) would be increased to 6.7nm RMS. From (f) to (g) in Fig. 2, the spot is linearly scaled along the major axis with constant VRR. We make the

Optics EXPRESS

similar manipulation from (b) to (e) with MRF spot (~13mm long), and the linear scale factor is same as that from (f) to (g). The residual errors (e) RMS is 1.6nm. The simulations indicate that the distribution-related sensitivity is proportional to the length of the spot. Hence, research on the material removal distribution profile is important in long-and-narrow Belt-MRF cases.

Previous research indicated that gap geometry can affect the removal function's shape [13,14], but a detailed analysis has not been performed. According to Preston's assumption [15], normal pressure is linearly related to the removal rate during a gradual changing process. We posited that in Belt-MRF the polishing gap can affect the removal function via the normal pressure distribution. Motivated by this assumption, we designed a "virtual ribbon" and built a model that describes its change in the polishing area. A linear gap was created between the belt and workpiece for maintaining a constant gap slope. Removal profiles in the long direction were obtained from experiments and model simulations. Our objective was to develop a method for predicting the removal spot by establishing a removal function model in terms of the gap slope.

In the rest of this paper, we present our removal distribution model for Belt-MRF based on Preston's equation (linear model). The concepts of gap slope and virtual ribbon are illustrated and the removal function model is introduced in Section 2. In Section 3, we simply introduce the mechanical structure of Belt-MRF, the pressure measuring system, and other experimental configurations. Using this setup, in Section 4.1, we demonstrate that measured and calculated pressure distributions coincide, and in the remainder of Section 4, we describe experimental validation of the calculated removal function.

2. Modeling the removal function for Belt-MRF

To the best of our knowledge, the present model is the first to address the removal rate distribution for Belt-MRF. This one-dimensional model describes the material removal rate distribution along the centerline of the polishing spot.

The model is based on the following classical equation by Preston [15]:

$$\Delta z(x) = \kappa \cdot p(x) \cdot v(x) \cdot \Delta t. \tag{1}$$

Here, Δz is the extent of material removal from the workpiece, κ is the Preston coefficient, p is the pressure between the ribbon and workpiece, v is the relative speed between the belt and the workpiece, and Δt is the dwell time. Because κ and v are thought to be constant along the flow direction in the polishing area, the material removal rate $\Delta z/\Delta t$ is linear in p.

The pressure is generated when the ribbon is dragged into the gap between the belt and the workpiece. Thus, the ribbon and the gap together affect the pressure in the MRF. The ribbon is determined after fixing all of the parameters except the gap for a certain process. Then, the pressure only depends on the gap. In this paper, we calculated the pressure by studying the relationship between it and the gap geometry, and then used Eq. (1) to predict the removal function.

Before studying the removal function model for Belt-MRF, we introduce the concepts of the gap slope and the virtual ribbon.

2.1 Gap slope

In the present Belt-MRF prototype, the magnet box has a flat bottom length of 60 mm and is connected with a two-arc part with a radius of 50 mm. In addition to the gap thickness, the gap distribution in Belt-MRF depends on the gap slope. The gap slope angle θ, shown in Fig. 3(a), is defined as the angle between the belt bottom and the workpiece along the x axis. Note that θ is negative when the belt bottom is in the clockwise direction of increasing x. Thus, the gap thickness can be written as

$$g(x) = g_0 + x \cdot k_g = g_0 + x \cdot \tan\theta. \tag{2}$$

Optics EXPRESS

Here, $g(x)$ is the gap thickness, g_0 is the initial gap thickness at the origin, and k_g, which is equal to $\tan\theta$, is the gap slope. As x increases from 0 mm to 60 mm, $g(x)$ increases linearly because k_g is constant. Except $x \in [0, 60]$ mm, the gap slope k_g is not constant.

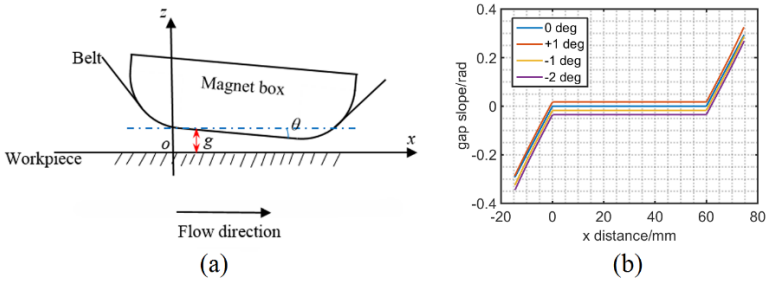

Fig. 3. The gap between the belt and the workpiece in Belt-MRF. (a) The geometrical relationship. (b) The gap slope distribution as θ varies.

Gap convergence is thought to be a necessary condition for material removal in MRF; here, the gap slope captures the gap convergence rate. In Fig. 3(a), it schematically shows that in the area of interest the gap thickness decreases gradually for negative θ and increases gradually for positive θ. As shown in Fig. 3(b), the gap slope profile cluster is calculated by the magnet box bottom slope and the workpiece slope. Each profile has two fold points at the edge of the modeling area, thus will probably introduce significant abnormality along the flow direction.

2.2 Virtual ribbon

The MR fluid ribbon plays an important role in determining the removal function in MRF. Of note, there are two interactions between the ribbon and the removal function. On one hand, the removal spot is not cut off at the gap minimum, and material removal extends beyond that point. On the other hand, the ribbon does not rebound after it is deformed by the gap in the magnetic field. Thus, the MR fluid is thought to be a viscoplastic fluid [16,17].

Here, we propose a virtual ribbon for describing how the MR fluid ribbon changes in the gap along the flow direction. Out of the polishing area, the virtual ribbon is equivalent to the real ribbon. The ribbon starts to experience deformation owing to the gap when the gap thickness is equal to the ribbon height (point *a* in Fig. 4). As the gap converges, the virtual ribbon is deformed at a certain rate. At the same time, the ribbon is transported by the belt, and the height of the virtual ribbon is larger than the gap thickness, for an arbitrary position. When the gap begins to diverge (point c in Fig. 4), the virtual ribbon is still deformed. As a result, no more material is removed when the virtual ribbon height is equal to the gap thickness.

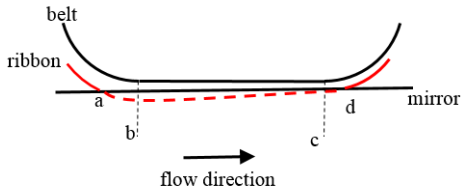

Fig. 4. Distribution of the virtual ribbon in Belt-MRF.

Optics EXPRESS

The height of the virtual ribbon with the gap thickness subtracted from it, is equal to the immersion depth of the ribbon, which is responsible for the normal pressure. It is this pressure that leads to the material removal. On the other hand, immersion depth in conventional MRF is defined as a single value calculated from the ribbon height and minimal gap thickness. Here, the height distribution for the virtual ribbon should be understood as an illustration of the immersion depth distribution for the entire polishing area.

2.3 Model of the removal rate distribution

As discussed above, the pressure can be calculated given the gap geometry. In conventional MRF, the removal function is relatively localized for the normal pressure to vary nonlinearly throughout the polishing area. In Belt-MRF, the removal spot is sufficiently large; the pressure varies linearly with distance throughout the main area of the gap. Thus, in the rest of this paper, the discussed area will be limited to the region in which the pressure behavior is linear.

The normal pressure distribution between the workpiece and the MR fluid ribbon is generated in a complex process that is not amenable to precise calculations. The MR fluid in the magnet field behaves solid-like, so the normal pressure can be calculated with elasto-mechanics. At the same time, the fluid also behaves liquid-like, so the hydrodynamics must be considered too. We decided to calculate the distribution of normal pressure using the concept of virtual ribbon. As what we concerned, the ribbon flow into the gap will create force and be affected by the force. Thus will simplify the modeling process. Two assumptions about the virtual ribbon and the pressure are made below to make the problem more tractable. First, we assumed that the rate of change of the virtual ribbon height is proportional to the normal pressure. It is reasonable that a larger normal pressure causes the ribbon height to decrease faster, which can be expressed as

$$\frac{dh(x)}{dx} = k_h(x)\cdot p(x), 0 \le x \le 60. \tag{3}$$

Here, $h(x)$ is the virtual ribbon height, $k_h(x)$ is the coefficient determined by the property of the ribbon, and $p(x)$ is the normal pressure. As the strength of the magnetic field B increases, the ribbon becomes stiffer; thus, less deformation is created by the same normal pressure. Thus, $k_h(x)$ is negatively correlated with B. The second assumption is that the normal pressure is proportional to the immersion depth of the virtual ribbon. The normal pressure is thought to be generated by the virtual immersion depth. The validity of the relationship had been proved for the macroscopic-scale MRF by Schinhaerl [18]. We assumed that this relationship is also valid at any point in the polishing area. The dependence can be expressed as

$$p(x) = k_p(x)\cdot\left(h(x) - g(x)\right). \tag{4}$$

Here, $g(x)$ is the gap thickness and $k_p(x)$ is the pressure coefficient. As the magnetic field's strength increases, the ribbon becomes stiffer, generating a larger normal pressure for the same immersion depth. Thus, $k_p(x)$ is positively correlated with B.

Combining Eqs. (3) and (4), the following equation is obtained for $h(x)$:

$$\frac{dh(x)}{dx} = k_h(x)\cdot p(x) = k_h(x)\cdot k_p(x)\cdot\left(h(x) - g(x)\right) = k(x)\cdot\left(h(x) - g(x)\right). \tag{5}$$

Here, $k(x)$ is a coefficient that describes how the virtual ribbon changes in the polishing area, and in our model this coefficient mainly depends on the magnetic field's strength B. According to the conclusion of Lambropoulos [19], the ribbon is insensitive to B for B above ~3000 G. Considering that the strength of the magnetic field generated by the permanent magnet used here was higher than 4000 G, and the field changed insignificantly along the

Optics EXPRESS

flow direction, the coefficients $k(x)$, $k_h(x)$, and $k_p(x)$ were considered to be constant in the area of interest; thus, we set k, k_h, and k_p.

From Eq. (5), we can calculate the virtual ribbon height $h(x)$:

$$h(x)=\frac{1}{k}\left(k_g-k_g\cdot e^{kx}+g_0\cdot k+(h_0-g_0)\cdot k\cdot e^{kx}+k_g\cdot k\cdot x\right). \tag{6}$$

Here, k_g is the gap slope, h_0 is the initial ribbon height, and g_0 is the initial gap thickness. The coefficient k is an important parameter of the present model. The value of k will be determined by experimentation.

Using Eqs. (4) and (6), the pressure can be written as,

$$p(x)=k_p\cdot\left(\left(h_0-g_0-\frac{k_g}{k}\right)\cdot e^{kx}+\frac{k_g}{k}\right). \tag{7}$$

According to Laun's research [20] for the normal pressure in MRF, it suggested that the normal plate-plate force is related with the magnet field strength B. Following a power law, we conclude that,

$$k_p\propto B^{2.4}. \tag{8}$$

If the gap and the magnet field strength changes slightly, k_p can be regarded as a constant in a certain parameter settings during process.

Upon Eq. (7), the removal rate distribution is calculated as,

$$\frac{\Delta z(x)}{\Delta t}=\kappa\cdot p(x)\cdot v(x)=\kappa\cdot v(x)\cdot k_p\cdot\left(\left(h_0-g_0-\frac{k_g}{k}\right)\cdot e^{kx}+\frac{k_g}{k}\right). \tag{9}$$

Generally speaking, the model indicates that the removal function changes as the gap geometry changes. Considering a linear gap between the flat magnet box bottom and the workpiece as an example, the gap geometry can be changed by changing the initial gap thickness and gap slope angle. Theoretically, the model suggests that removal functions with various shapes can be designed for Belt-MRF.

2.4 Simulated removal function

For any given scenario, the removal function is determined by the four parameters h_0, g_0, k_g, and k. The initial gap thickness g_0 and the gap slope k_g can be measured, while the initial virtual ribbon height h_0 and the coefficient k remain to be determined. In the following simulations of removal function, we set g_0 to 2.5 mm, which is a moderate value.

First, the gap slope k_g was set to –0.007 (θ = –0.4°), and we calculated the removal function considering h_0 to be 3.0 mm, and treating k as an unknown coefficient (typically, k = 10^{-1} ~10^{-3}). The resulting simulated removal functions, which is calculated from Eq. (9), are plotted in Fig. 5. The normalized removal function and pressure were calculated using normalization factor as the value at (x = 0) hereinafter.

Optics EXPRESS

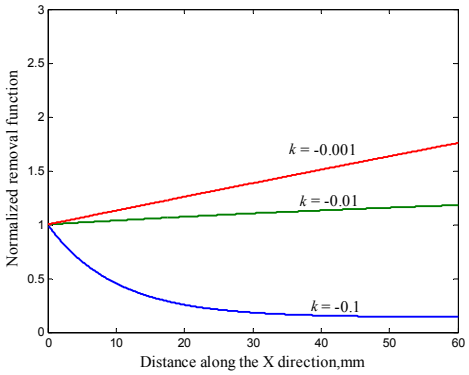

Fig. 5. Simulated normalized removal functions vs. the x distance, for different k. Parameters: $h_0 = 3.0$ mm and $\theta = -0.4°$.

Next, we calculated removal functions for $k = -0.01$ and by varying h_0 from 2.6 mm to 3.0 mm. The removal functions are shown in Fig. 6.

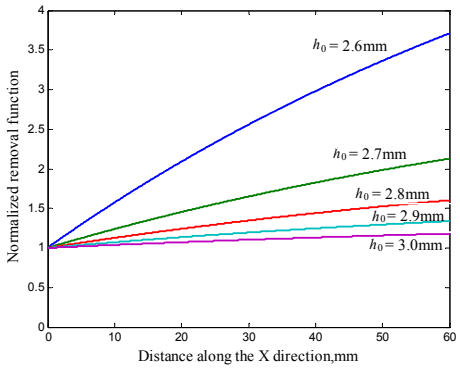

Fig. 6. Simulated normalized removal functions vs. the x distance, for different h_0. Parameters: $k = -0.01$ and $\theta = -0.4°$.

Simulated removal functions for different slope angles are shown in Fig. 7. It shows that the removal function strongly depends on the slope angle θ, which allows to calculate k and h_0 by considering removal functions for different slope angles.

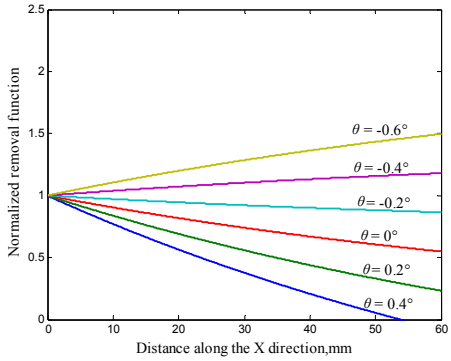

Fig. 7. Simulated normalized removal functions, vs. the x distance, for different θ. Other parameters: $k = -0.01$ and $h_0 = 3.0$ mm.

Optics EXPRESS

There are two modeling parameters (k, and h_0) remain to be unknown. Thus, knowing one removal function is not sufficient for determining the values of these parameters; at least two removal functions, for different slope angles, are needed. It is reasonable that when the initial gap thickness g_0 is constant, and when k_g changes weakly, the initial virtual ribbon height h_0 and the ribbon coefficient k will also be constant.

3. Experimental setup

3.1 Experimental configuration

Experiments were conducted using a self-produced Belt-MRF prototype, shown in Fig. 8. The MR fluid used in the experiments had been proven to be highly efficient and stable, guaranteeing the credibility of the polishing spot [21].

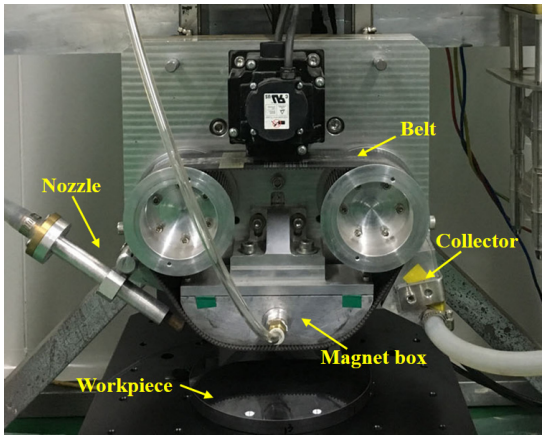

Fig. 8. Belt-MRF prototype.

3.2 Position of the removal spot calibration

To study the distribution of the removal rate in the gap, it is necessary to calibrate the position of the removal spot relative to the origin of the workpiece's coordinate system.

By marking two locations on the workpiece and taking pictures of the marks and the magnet box, we obtained the relative positions of the marks and the magnet box. This allowed to determine precisely the location of the removal spot in the workpiece's coordinate system.

3.3 Gap thickness and gap slope calibration

The gap thickness in conventional MRF is decided by the minimal gap at the bottom of the wheel. On the other hand, owing to the flat bottom of the magnet box in Belt-MRF, the initial gap thickness g_0 is defined as the vertical distance between the belt and the workpiece at the origin (OO' in Fig. 9).

A measuring arm was used for measuring the slope angle in the x direction (flow direction) and y direction. The result of this measurement was replicable within ± 0.025°.

Optics EXPRESS

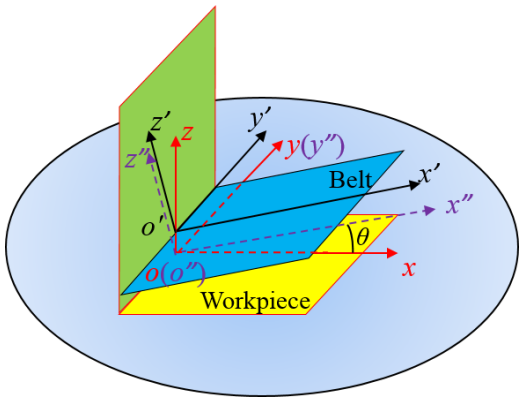

Fig. 9. Calibration of the gap thickness and gap slope.

The slope angle in the *y* direction was adjusted to be 0°, so as to ensure the symmetry of the removal function in that direction. After the gap thickness and its slope were calibrated, the gap geometry between the workpiece and the belt was uniquely determined.

3.4 Pressure distribution test system

The normal pressure distribution in the polishing area was measured using the Tekscan® system. The sensor that we used had a lateral resolution of 2.5 mm and its thickness was 0.3 mm [22]. The sensor was adhered to the surface of a flat mirror, shown in Fig. 10, making the setup similar to that of the removal function experiment.

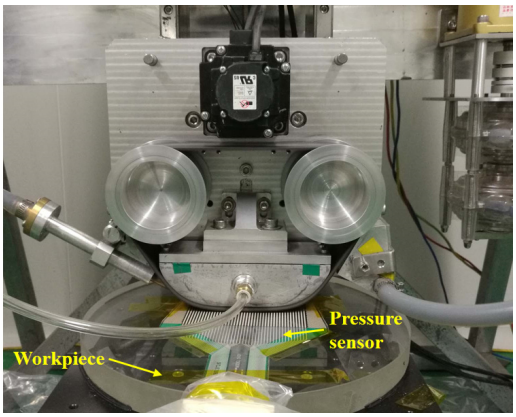

Fig. 10. Configuration of the normal pressure test.

4. Experimental demonstration of the removal function model

We performed one experiment to validate the calculated pressure, and three additional experiments to measure the removal function. The corresponding experimental conditions are listed in Table 1.

Optics EXPRESS

Table 1. Experimental conditions.

Experiment	No.	1&2	3	4
General	Run time	20 s	20 s	20 s
	MR fluid abrasive	Nano-diamond	Nano-diamond	Nano-diamond
Workpiece	Size	⌀150 mm	⌀150 mm	⌀150 mm
	Material	RB-SiC (pressure tested on K9 in #1)	RB-SiC	RB-SiC
	Initial surface error	14 nm RMS	14 nm RMS	13 nm RMS
Parameters	Deliver pump speed	156 rpm	156 rpm	156 rpm
	Discharge pump speed	200 rpm	200 rpm	200 rpm
	Belt velocity	1 m/s	1 m/s	1 m/s
	Air pressure*	3.5 bar	3.5 bar	3.5 bar
	Gap thickness	2.5 mm	2.5 mm	2.0 mm to 3.5 mm
	Gap slope	–0.4° and –0.6°	–0.6° to 0.4°	–0.2°

* The pressure of the air which flows into the magnet box to reduce the friction between its bottom and the belt.

4.1 Experiment 1: distribution of pressure in Belt-MRF

The distribution of normal pressure was measured in the first experiment for the gap thickness of 2.5 mm and for the slope angles of –0.4° and –0.6°, which are moderate values.

According to the experimental results and the model in Eq. (7), k and h_0 were calculated to be –0.01 and 2.8 mm respectively. The calculated and measured pressure distributions are plotted in Fig. 11. In this plot, the pressure and the removal rate are normalized by their values at the origin, which facilitates comparisons across simulations and experimental results.

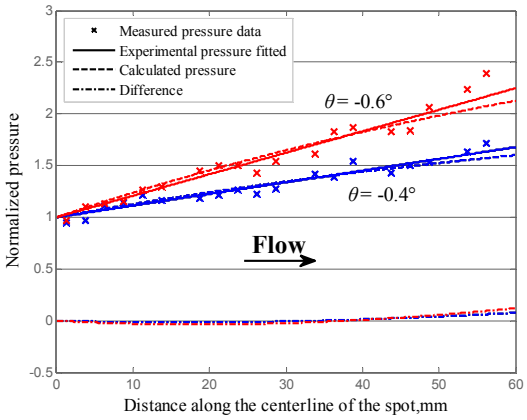

Fig. 11. Calculated and measured pressure distributions, for the slope angles of –0.4° and –0.6°.

For both slope angles, the calculated pressure distributions were in a good agreement with the measured ones. The measured pressure scaled nearly linearly with distance. The largest difference between the calculated and measured pressures was under 7%. These results confirm that the pressure equation is adequate for calculating the distribution of pressure in Belt-MRF.

Optics EXPRESS

4.2 Experiment 2: validation of removal rate distribution

The removal function experiment was conducted using the same parameters as those that were used in the pressure experiment. The slope angles, same as for the pressure experiment, were −0.4° and −0.6°. All of the centerline profiles in this paper are obtained as shown in Fig. 12(b). The simulated removal profiles were obtained according to Eq. (8) and then compared with the experimental results in Fig. 13.

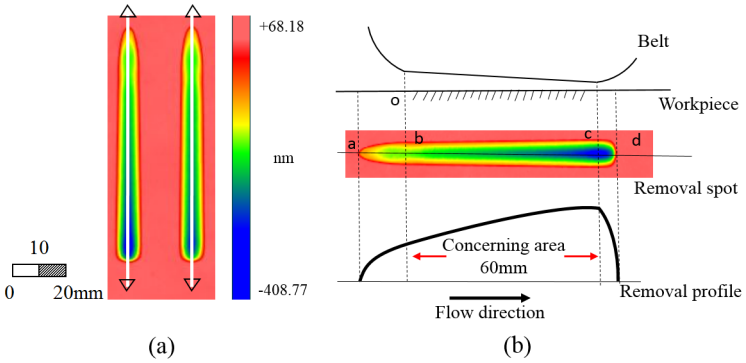

Fig. 12. Experimental results. (a) Removal spots, for −0.6° (left), and −0.4° (right). (b) Schematic of the spot centerline profile.

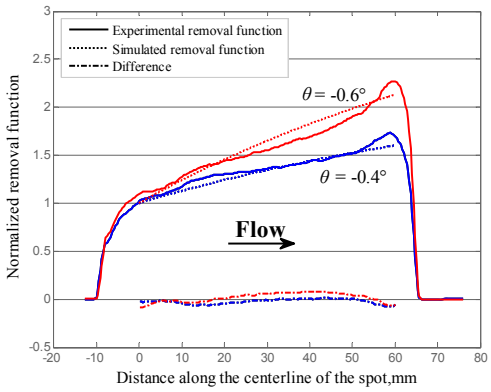

Fig. 13. Experimental and simulated removal function centerline profiles, for the slope angles of −0.4° and −0.6°.

The above results reveal a good agreement between simulated and experimentally measured removal functions. The simulated and experimentally measured functions deviate only at the edges of the area of interest, and the deviation is under 8%. It is plausible to assume that the edges of the area of interest separate between linear and nonlinear gap regimes. Thus, the above results demonstrate that it is possible to analyze the removal function in the main area of Belt-MRF, which allows to predict the normal pressure distribution. In general, as long as two removal functions can be obtained for two slope angles, the unknown parameters in the removal function model can be calculated, allowing to predict the removal function for other slope angles.

4.3 Experiment 3: removal functions for different slope angles

To determine the model's predictive power, a third experiment was performed, for six different slope angles. The experimental centerline spot profiles and the simulated removal profiles, obtained using the determined h_0 and k, are plotted and compared in Fig. 14.

Optics EXPRESS

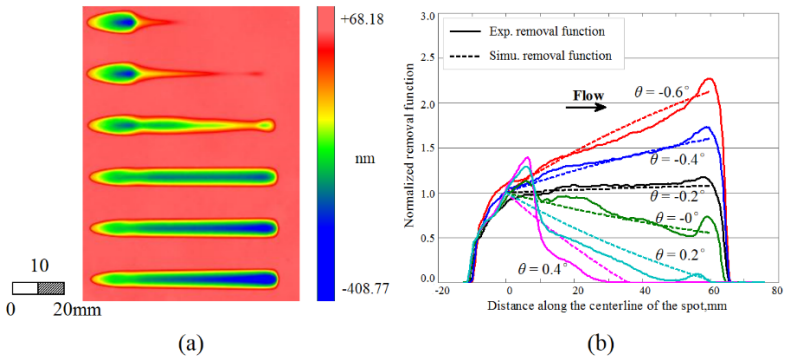

Fig. 14. Removal spots and model simulation results, for different slope angles. (a) Removal spots, for slope angles ranging from 0.4° (top) to –0.6° (bottom). (b) Comparison of experimental and simulated profiles.

As shown in Fig. 14(a), there is a necking of each removal profile. At $x = 0$, the gap slope changes discontinuously with the magnet box bottom changing from a cylinder to a plane. While the removal function in the modeling area, where $x \in [0, 60]$ mm, is linear as the model predicted. In Fig. 14(b), for negative slope angles the simulated removal functions are in a good agreement with the experimentally measured ones. Yet, for positive slope angles, the simulated removal functions deviate from the experimentally measured ones.

The VRR and PRR (peak removal rate) shown below were calculated by the removal spots measured using a ZYGO® interferometer. The spot polishing time was controlled to ensure all data be collected.

Table 2. VRR and PRR of the removal function, for different slope angles.

Gap slope angle θ (°)	Initial gap thickness g_0 (mm)	VRR (mm^3/min)	PRR (μm/min)
0.4	2.5	0.083	1.133
0.2	2.5	0.094	0.994
0	2.5	0.176	0.867
–0.2	2.5	0.277	0.879
–0.4	2.5	0.294	1.112
–0.6	2.5	0.306	1.317

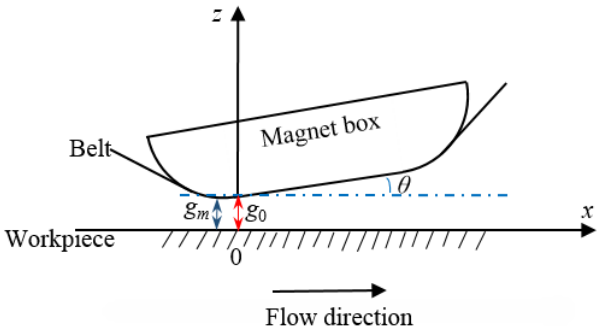

Fig. 15. Minimal gap g_m for positive slope angles θ.

From the results in Table 2 and Fig. 14(b), the PRR increases as the slope angle increases from 0° to 0.4°. From Fig. 15 it can be inferred that the minimal gap thickness g_m decreases while the initial gap thickness g_0 is fixed at 2.5 mm during the experiment. Owing to this, the initial location of the virtual ribbon changes significantly as the slope angle increases above

Optics EXPRESS

0°. Thus, simulated removal functions are not consistent with their experimental counterparts for positive angles, as is also clear from Fig. 14(b). In line with the above discussion, for positive slope angles θ the gap between the belt and the workpiece diverges in the main area. Thus, the removal rate distribution quickly drops to zero as the gap starts to diverge.

4.4 Experiment 4: removal functions for different gap thicknesses

Another removal function experiment was performed for different gap thicknesses, setting the slope angle to –0.2° (see Table 3). The results of this experiment are shown in Fig. 15.

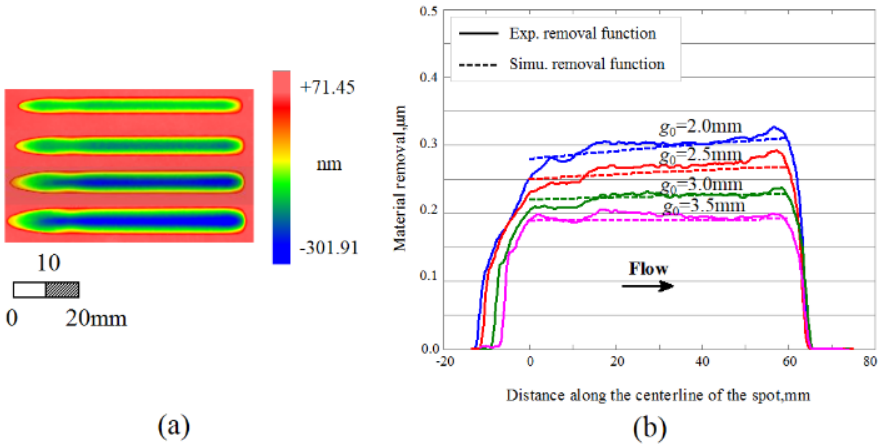

Fig. 16. Removal spots and model simulation results, for different initial gap thicknesses. (a) Removal spots, for gap thicknesses ranging from 3.5 mm (top) to 2.0 mm (bottom). (b) Comparison of experimental and simulated profiles.

Table 3. VRR and PRR of the removal function, for different gap thicknesses.

Gap slope angle θ (°)	Initial gap thickness g_0 (mm)	VRR (mm^3/min)	PRR (μm/min)
–0.2	2.00	0.341	0.998
–0.2	2.50	0.277	0.879
–0.2	3.00	0.202	0.728
–0.2	3.50	0.143	0.617

The curve cluster in Fig. 16(b) suggests that the removal rate distributions are similar for different gap thicknesses. As discussed in Section 2.4, h_0 and k change with g_0. The value of h_0 was calculated according to the magnitude of the removal rate at the origin, following which Eq. (8) was used for obtaining the coefficient k from the removal profile. The values of h_0 and k were calculated for different gap thicknesses and are listed in Table 4.

Table 4. Parameters of the removal function model.

Initial gap thickness g_0 (mm)	Initial ribbon height h_0 (mm)	Model coefficient k (mm^{-1})
2.0	2.34	–0.008
2.5	2.8	–0.01
3.0	3.27	–0.012
3.5	3.73	–0.015

Optics EXPRESS

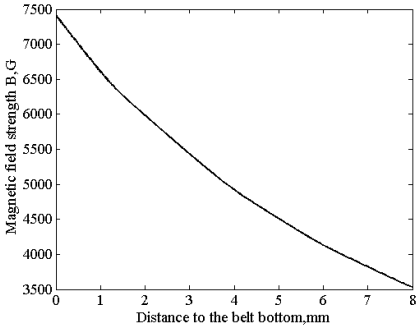

Fig. 17. Intensity of the magnetic field B along the vertical direction from the belt bottom.

Based on the results in Table 4 we conclude that as g_0 changes from 2.0 mm to 3.5 mm, the coefficient k changes as well. But, it is important to realize that the value of k is ~–0.01. Considering that the average strength of the magnetic field, which was acquired by the Gauss meter, also changes as shown in Fig. 17, it is reasonable to assume that the absolute value of k is negatively correlated with B in the area of interest, similar to the discussion in Section 2.3. To study the relationship between k and B, it would be necessary to vary B while keeping other parameters constant. This can be achieved using electromagnets.

5. Conclusions

Previous research has revealed that the distribution of the MRF removal rate depends on the gap geometry. Here, we studied the relationship between the gap profile and material removal profile; thus, a linear gap was created by designing a magnet box with a flat bottom in Belt-MRF. We sought to establish a removal rate distribution model that would allow to predict the removal function from the gap profile.

Experimental validations of pressure and removal function were successfully performed, and the experimental measurements were consistent with the results of their corresponding theoretical calculations. The measured pressure coincided with the calculated pressure. The simulated removal function was in a good agreement with the experimentally measured one.

Under our experimental conditions, the coefficient k was ~–0.01. Note that this coefficient determines the behavior of the MR fluid ribbon in the magnetic field; thus, k depends on the magnetic field strength, MR fluid, initial ribbon configuration, and material properties, to name a few. Additional work is needed to determine how k changes with experimental conditions. The necking at fold points of the gap slope distribution will also be discussed particularly in the future.

In general, specific gap geometries in Belt-MRF could be obtained by changing the shape of the magnet box's bottom, which could be helpful for determining the relationship between the removal rate distribution and the gap convergence rate, as discussed in this paper. Furthermore, the proposed approach allows to design removal function profiles to a certain extent.

Funding

National Natural Science Foundation of China (NSFC) (61605202, 61210015).